Title
Stripes developed at the strong limit of nematicity in FeSe film

Journal
Nature Physics, 13(10)

ISSN
1745-2473

Authors
Li, Wei
Zhang, Yan
Deng, Peng
et al.

Publication Date
2017-10-01

DOI
10.1038/nphys4186

Peer reviewed

Stripes Developed at the Strong Limit of Nematicity in FeSe Film

Wei Li[1,2,3*], Yan Zhang[2,3,4,5], Peng Deng[1], Zhilin Xu[1], S.-K. Mo[4], Ming Yi[3], Hao Ding[1], M. Hashimoto[6], R. G. Moore[3], D.-H. Lu[6], Xi Chen[1,2*], Z.-X. Shen[3,7*], and Qi-Kun Xue[1,2]

[1]*State Key Laboratory of Low-Dimensional Quantum Physics, Department of Physics, Tsinghua University, Beijing 100084, China*

[2]*Collaborative Innovation Center of Quantum Matter, Beijing 100084, China*

[3]*Stanford Institute for Materials and Energy Sciences, SLAC National Accelerator Laboratory and Stanford University, Menlo Park, California 94025, USA*

[4]*Advanced Light Source, Lawrence Berkeley National Lab, Berkeley, California 94720, USA*

[5]*International Center for Quantum Materials, School of Physics, Peking University, Beijing 100871, China*

[6]*Stanford Synchrotron Radiation Lightsource, SLAC National Accelerator Laboratory, Menlo Park, California 94025, USA*

[7]*Departments of Physics and Applied Physics, and Geballe Laboratory for Advanced Materials, Stanford University, Stanford, California 94305, USA*

*To whom correspondence should be addressed: weili83@tsinghua.edu.cn, zxshen@stanford.edu and xc@mail.tsinghua.edu.cn

Superconductivity in one unit cell FeSe film on $SrTiO_3$ has attracted enormous attentions[1-5], due to its impressive enhancement of superconductivity[1], novel Fermi surface topology[2-5], extreme two-dimensionality as well as the possibility of phonon-enhanced electron pairing[1,5]. However, the electronic behaviors of FeSe films on $SrTiO_3$ show extraordinary dichotomy as the superconductivity is drastically suppressed and strong nematicity develops for the film thicker than one unit cell. On the other hand, the absence of long-range magnetism despite large local magnetic moment in bulk FeSe, makes it an exception among the iron-based superconductors. Here we report on low-temperature scanning tunneling microscopy studies of the multilayer FeSe films grown by molecular beam epitaxy. We find a stripe-type charge ordering instability, which develops beneath the nematic state. The charge ordering is visible and pinned in the vicinity of impurities. The emergence of stripe-type charge ordering at the strong limit of nematicity may indicate a magnetic fluctuation with a rather small wave vector, competing with the ordinary collinear antiferromagnetic order in the multilayer FeSe films. The existence of stripes in iron-based superconductor that resemble the stripe order in cuprates not only suggests the importance of electronic anisotropy and correlation, but also provide a platform to reveal the complex interactions between nematicity, charge ordering, magnetism and superconductivity in high-temperature superconductors.

Nematicity[6] in iron-based superconductors, defined as broken rotational symmetry of the tetragonal lattice (the nonequivalence of a- and b-axis in Fig. 1a), has been manifested in various studies[7-14], such as large in-plane anisotropy in neutron scattering[7] and transport measurements[8], unidirectional nanostructures in scanning tunneling microscopy (STM)[9] and lifting of orbital degeneracy of d_{xz}/d_{yz} bands in angle-resolved photoemission spectroscopy (ARPES)[11]. Although the d_{xz}/d_{yz} bands splitting has been observed in both FeSe single crystals[15, 16, 17] (bulk FeSe) and FeSe films grown on $SrTiO_3$ (FeSe/STO)[18], the strength of nematicity in FeSe/STO is much larger than that in bulk FeSe reflected in the much higher nematic phase transition temperature in FeSe/STO[18]. Consequently, superconductivity does not recover in the multilayer FeSe/STO even with thickness of 30 unit cell (UC), while bulk FeSe[19] becomes superconducting around 8 K. No evidence shows that nematicity hinders the emergence of superconductivity in FeSe (bulk FeSe exhibits superconductivity as well as nematicity), conversely, it has been proposed to cause enhancement of

electrons pairing to certain extend[3]. Therefore, there might exist another hidden order competing with superconductivity in multilayer FeSe/STO.

FeSe exhibits intriguing magnetic properties as well. For example, although long-range magnetic order is absent in bulk FeSe with rather large local magnetic moment, the commonly found collinear antiferromagnetism emerges rapidly under high pressure[20-22]. This indicates that the carriers of FeSe are in a delicate balance in spin channel, which may also account for the potential high-temperature electrons pairing. Here we combine molecular beam epitaxy (MBE) and STM together to reveal the mystery of FeSe.

Figure 1b shows a typical STM topographic image of a 30 UC FeSe film grown on STO. The surface is divided into multiple domains with maze-like patterns, which are spread throughout the whole sample surface and could be attributed to the boundaries between two perpendicular nematic domains. Impurities (dark dots in Fig. 1b and c) are introduced as scattering centers to reveal the electronic interactions in FeSe film. Most of the impurities present a dumbbell-shaped structure[23,24] and are likely the Fe-vacancies[25] underneath the Se-terminated surface (Fig. 1c). The boundaries are highlighted by orange dashed lines. An intriguing behavior is that stripe pattern could be induced in the vicinity of the impurities. The stripes are unidirectional within each domain, while the orientation of the stripes (marked by white arrows) rotates 90° when crossing the domain boundary. The existence of the stripes as well as the domains indicates the two-fold symmetry of the underlying electronic structure, and provide the direct evidence of the existence of nematicity in FeSe/STO. Hereafter the boundaries will be referred as C_2 domain walls, which is also the fingerprints of nematicity in FeSe films studied by STM. The typical width of the domain wall is ~ 4 nm (supplementary Note 1). High resolution STM topographic image (inset of Fig. 1c) exhibits the Se-Se lattice as well as the stripes simultaneously, from which the periodicity of ~ 1.9 nm and orientation (along diagonal direction of Se-Se lattice, i.e. the direction of Fe-Fe lattice) of the stripes are determined.

The stripe feature is robust and could be clearly resolved over a rather wide energy range in STM topography. As shown in Fig. 2a-d, stripes are pinned by four dumbbell-shaped impurities, which act as landmarks as well to inspect the details of the stripes. A large number of impurities have been inspected and the induced stripes are all identical, therefore, the phase of the stripes is pinned by the impurities. Arrows in Fig. 2 indicate the stripes between two impurities. With various bias voltages, the

periodicity of stripe is unchanged (static), while its phase changes by 180° under -30 mV (denoted by colors of the arrows). The above behavior of the stripes is reminiscent of charge ordering in charge density waves (CDW) materials. Alternative explanation for the stripes is quasiparticle interference (QPI) induced by impurities, which reflects the bands structure information of the system. However, it is unlikely because of the following reasons. STM topographic image represents the convolution of density of states (DOS) within an energy range from the Fermi level (E_F) to the sampled bias voltage, and thus usually smears out any QPI feature in real space due to drastic variation of energy dependent scattering wave vectors (especially at high bias voltages).

The charge ordering (CO) origin of the stripes is further supported by *dI/dV* maps as shown in Fig. 3. We focus on the area within the white dashed line in Fig. 2d, where two impurities as well as the induced stripe patterns are included. *dI/dV* map shows spatial distribution of DOS at a specific energy, from which the scattering wave vectors could be extracted. Sweeping the bias voltage *V (*energy*)*, a series of energy-dependent wave vectors are mapped out. This is the basic idea of QPI method, and the obtained wave vectors usually arise from the inter- or intra-band scattering of quasiparticles. The most striking feature in *dI/dV* maps (Fig. 3) is the static (non-dispersive) stripe pattern persisting within an extremely large energy range from -200 meV to 500 meV. This is a decisive evidence of CO rather than QPI origin of the stripes, since no band near E_F has such a large band width in FeSe. Meanwhile, the contribution of intra-band scattering (QPI) near E_F can also be observed (highlighted by orange arcs) in *dI/dV* maps (Fig. 3i-m), corresponding to a hole-like band (see the band structure and wave vector marked by green arrows in Fig. S4) near E_F. The unidirectional QPI features at negative bias voltages are perpendicular to the orientation of the stripes. Based on that, we determine that the orientation of the stripes is along the a-axis (supplementary Note 2 and Note 3).

We now turn to discuss the driving force of the CO and its connection with nematicity. Fig. 4a shows C_2 domain walls at 77 K, indicating the persistence of nematicity at this temperature. The C_2 domain walls gradually disappear at elevated temperatures (Fig. 4b-d) and the nematic transition (T^*) happens around 120 K, consistent with our previous ARPES measurement[18]. However, the stripes are absent at 77 K (see the zoom-in topography in Fig. 4e), indicating a new temperature scale for the development of CO. Temperature-dependent measurement of the stripes (Fig.

4e-h) demonstrates the transition temperature of CO (T_{CO}) is around 60 K. More importantly, the periodicity of the stripes is not sensitive to temperature once formed (see the highlighted area marked by white arrows and red dashed lines in Fig. 4f-h at 60 K, 45 K and 4 K, respectively).

Figure 4i is a phase diagram summarized from the temperature-dependent measurements of the stripes and nematicity. The nematicity appears at 120 K and is gradually enhanced at lower temperature, then the CO develops around 60 K. Given the facts that the stripes emerge within the nematic phase and the absence of stripes in bulk FeSe that exhibits weaker nematicity[17]. The strength of nematicity hence is crucial to the formation of the stripes. An instinctive picture to understand the nematicity induced CO is: the band width of d_{xz} band becomes wider while d_{yz} band becomes narrower (Fig. S4) with larger anisotropy (nematicity)[18], then the electrons tend to be more itinerant along one direction but more localized (to stripe) along the perpendicular one. A straightforward explanation of the CO is the Fermi surface nesting picture. However, it is unlikely due to the temperature independence of the stripes. At elevated temperatures, the strength of the nematicity as well as the bands splitting size decrease, giving rise to significant variations of the Fermi surfaces[18], which cannot contribute a temperature independent wave vector in momentum space.

Besides nematicity, another essential ingredient to induce the stripes is the impurity, since the CO is always observed in the vicinity of impurities. The correlation length of the induced stripes is ~ 2.1 nm (Note 4 in supplementary materials). The dumbbell-shaped impurities are likely the Fe-vacancies, commonly found in bulk FeSe[23-25]. They have two possible orientations along the Se-Se lattice directions which are perpendicular to each other, representing the missing of one Fe atom (Fe-vacancy) in Fe-Fe lattice (see in Fig. 5c and d). One role of the iron-vacancy is to further break the two-fold symmetry[26], and the strength of nematicity therefore is enhanced locally, which promotes the emergence of the stripes.

dI/dV spectra near the stripes do not show any gap-like features (Fig. S6 and supplementary Note 5), suggesting a partial band gap opening in momentum space. Due to the small amount of impurities and the limited areas with stripes in FeSe film, ARPES that takes the average of signal from an area of tens of square microns, could not reveal the band folding and gap opening stemming from the CO. The impurity states (supplementary Note 5) are strongly distorted by interacting with the CO. As shown in Fig. 5a and b, the directions of the dumbbell-shapes (denoted by red dashed

lines) show obvious deviation of larger than 10° from that of the Se-Se lattice (yellow dashed lines). The impurity states interact with the CO and tend to align with the stripes, giving rise to the observed deviation. At 77 K, with the absence of the stripes, the deviation disappears and the two impurities are perpendicular to each other again (Fig. 5c).

The appearance of stripes near the Fe-vacancy indicates a possible magnetic fluctuation in Fe-plane. The impurities help to pin the fluctuation, which is then captured by STM tip in charge channel. Long-range magnetic order is absent but the collinear AFM emerges rapidly under high pressure in bulk FeSe[20-22], indicating that there might be two comparable competing orders in spin channel at ambient pressure. A tiny change of the lattice constant may break the balance. Positive pressure to FeSe causes emergence of collinear AFM[20-22]. Conversely, tensile stress is applied when FeSe is grown on STO, equivalent to apply a negative pressure to the system. Therefore, the other side of the pressure-related phase diagram of FeSe is reached, within which the correlation of the whole system is enhanced and the other magnetic order wins. A magnetic fluctuation with a rather small $q \sim \pi/5$ is predicted in bulk FeSe[27], quantitatively comparable with the periodicity of the observed stripes. We therefore attribute the observed stripes to the origin of a charge ordering induced by the magnetic fluctuation. The two possible fluctuations in spin channel might be crucial to understand the unique properties of FeSe, such as the magnetism under pressure[20-22] and electron pairing at rather high temperatures[1, 20].

The existence of CO instability also provides a natural explanation of the suppression of superconductivity in multilayer FeSe/STO. Commonly happened in other materials, such as cuprates and transition metal dichalcogenides, superconductivity always competes with CO. Besides the impurities we discussed above, the widespread C_2 domain walls induce the stripes as well where the domain walls are aligned with the intrinsic stripe directions (Fig. S7). This could play a more important role to break the long-range coherence of cooper pairs in multilayer FeSe films.

The stripe-type charge ordering in iron-based superconductor resembles that in cuprates and suggests the importance of electronic anisotropy and correlation. Our findings shed new light on understanding the complex relationship between nematicity, charge ordering, magnetism and superconductivity in high-temperature superconductors.

Methods

FeSe films were grown on Nb-doped (0.05% wt) $SrTiO_3$ (100). TiO_2 terminated atomically flat surfaces were prepared by degassing at 450 °C for one hour and subsequently annealing at 1100 °C for 20 min. For the FeSe films for STM measurements, high purity Fe (99.995%) and Se (99.9999%) were evaporated from two standard Knudsen cells. The growth was carried out under Se-rich condition with a nominal Se/Fe flux ratio of ~20. For the FeSe film for ARPES measurements, an e-beam cell and a thermal cracker effusion cell were used to evaporate Fe and Se, respectively. The Se/Fe flux ratio was set between 3~4. Substrate temperatures were kept at 370 °C for both growth methods. The as-grown FeSe films were subsequently annealed at 400 °C for several hours to remove the excess Se. Both films are of comparable high quality judging from the reflection high-energy electron diffraction (RHEED) patterns, STM and ARPES results.

To introduce iron-vacancies as the scattering centers for the STM studies. The as-grown FeSe films were annealed at a lower temperature ~ 380 °C, and low density of iron-vacancies could be obtained in the films.

In-situ STM experiments were conducted in an ultra-high vacuum (UHV) low temperature (4 K) STM equipped with an MBE chamber for film growth (Unisoku). A polycrystalline PtIr STM tip was used and characterized on Ag island before STM experiments.

ARPES measurements were performed at the Stanford Synchrotron Radiation Lightsource Beamline (SSRL) 5-4 and the Advanced Light Source (ALS) Beamline 10.1 at 21 K. The as-grown FeSe films were transported to ARPES chamber for SSRL measurements under UHV via a vacuum suit-case that is pumped by an ion pump. The FeSe samples measured in ALS were capped with 20 nm Se as protecting layers. The protecting layers were de-capped by carefully annealing the samples at 400 °C and monitored by RHEED. The recovery of the bright and sharp RHEED patterns during the heating procedures indicated the clean surface of FeSe films. The samples measured in SSRL and ALS show consistent band structures.

Data Availability. The data that support the plots within this paper and other findings of this study are available from the corresponding author upon reasonable

request.

References

1. Wang, Q. Y. *et al*. Interface induced high temperature superconductivity in single unit-cell FeSe films on $SrTiO_3$. *Chin. Phys. Lett*. **29**, 037402 (2012).

2. Liu, D. F. *et al*. Electronic origin of high-temperature superconductivity in single-layer FeSe superconductor. *Nat. Commun.* **3**, 931 (2012).

3. Tan, S.Y. *et al*. Interface-induced superconductivity and strain-dependent spin density waves in FeSe/$SrTiO_3$ thin films. *Nat. Mater*. **12**, 634 (2013).

4. He, S. L. *et al*. Phase diagram and high temperature superconductivity at 65K in tuning carrier concentration of single-layer FeSe films. *Nat. Mater*. **12**, 605 (2013).

5. Lee, J. J. *et al*. Interfacial mode coupling as the origin of the enhancement of Tc in FeSe films on $SrTiO_3$. *Nature* ***515***, 245 (2014).

6. Kivelson, S. A., Fradkin, E. & Emery, V. J. Electronic liquid-crystal phases of a doped Mott insulator. *Nature* **393**, 550–553 (1998).

7. Zhao, J. *et al*. Spin waves and magnetic exchange interactions in $CaFe_2As_2$. *Nat. Phys.* **5**, 555-560 (2009).

8. Chu, J. H. *et al*. In-plane resistivity anisotropy in an underdoped iron arsenide superconductor. *Science* **329**, 824-826 (2010).

9. T.-M. Chuang *et al.* Nematic electronic structure in the "parent" state of the iron-based superconductor $Ca(Fe_{1-x}Co_x)_2As_2$. *Science* **327**, 181 (2010).

10. Kasahara, S. *et al*. Electronic nematicity above the structural and superconducting transition in $BaFe_2(As_{1-x}P_x)_2$. *Nature* **486**, 382-385 (2012).

11. Yi, M. *et al*. Symmetry-breaking orbital anisotropy observed for detwinned $Ba(Fe_{1-x}Co_x)_2As_2$ above the spin density wave transition. *Proc. Natl Acad. Sci. USA* **108**, 6878-6883 (2011).

12. Rosenthal, E. P. *et al*. Visualization of electron nematicity and unidirectional antiferroic fluctuations at high temperatures in NaFeAs. *Nat. Phys.* **10**, 225–232 (2014).

13. Tanatar, M. A. *et al*. Uniaxial-strain mechanical detwinning of $CaFe_2As_2$ and $BaFe_2As_2$ crystals: Optical and transport study. *Phys. Rev. B* **81**, 184508 (2010).

14. Lee, C.-C., Yin, W. G. & Ku, W. Ferro-orbital order and strong magnetic anisotropy in the parent compounds of iron-pnictide superconductors. *Phys. Rev. Lett.* **103**, 267001 (2009).

15. Nakayama, K. *et al*. Reconstruction of Band Structure Induced by Electronic Nematicity in an FeSe Superconductor. *Phys. Rev. Lett*. **113**, 237001 (2014).

16. Borisenko, S. V. *et al*. Direct observation of spin–orbit coupling in iron-based

superconductors. *Nat. Phys.* **12**, 311-317 (2016).
17. Watson, M. D. *et al*. Evidence for unidirectional nematic bond ordering in FeSe. *Phys. Rev. B* **94**, 201107(R) (2016).
18. Zhang, Y. *et al*. Distinctive orbital anisotropy observed in the nematic state of a FeSe thin film. *Phys. Rev. B* **94**, 115153 (2016).
19. Hsu, F. C. *et al*. Superconductivity in the PbO-type structure α-FeSe. P*roc. Natl. Acad. Sci. U.S.A.* **105**, 14262 (2008).
20. Bendele, M. *et al.* Coexistence of superconductivity and magnetism in $FeSe_{1-x}$ under pressure. *Phys. Rev. B* **85**, 064517 (2012).
21. Sun, J. P. *et al*. Dome-shaped magnetic order competing with high-temperature superconductivity at high pressures in FeSe. *Nat. Commun.* **7**, 12146 (2016).
22. Kothapalli, K. *et al*. Strong cooperative coupling of pressure-induced magnetic order and nematicity in FeSe. *Nat. Commun.* **7**, 12728 (2016).
23. Song, C.-L. *et al.* Suppression of superconductivity by twin boundaries in FeSe. *Phys. Rev. Lett.* **109**, 137004 (2012).
24. Kasahara, S. *et al*. Field-induced superconducting phase of FeSe in the BCS-BEC cross-over. P*roc. Natl. Acad. Sci. U.S.A.* **111**, 16309 (2014).
25. Huang, D. *et al*. Dumbbell Defects in FeSe Films: A Scanning Tunneling Microscopy and First-Principles Investigation. *Nano Letters* **16**, 4224 (2016).
26. Inoue, Yoshio, Yamakawa, Youichi & Kontani, Hiroshi. Impurity-induced electronic nematic state and C_2-symmetric nanostructures in iron pnictide superconductors. *Phys. Rev. B* **85**, 224506 (2012).
27. Tam, Y.-T., Yao, D.-X. & Wei, Ku. Itinerancy-enhanced quantum fluctuation of magnetic moments in iron-based superconductors. *Phys. Rev. Lett.* **115**, 117001 (2015).

Acknowledgements

We thank T, Li, H. Yao and J. P. Hu for discussions. STM work was supported by the National Science Foundation (No. 11674191) and Ministry of Science and Technology of China (No. 2016YFA0301002). W. Li was also supported by Beijing Young Talents Plan. ALS and SSRL are operated by the Office of Basic Energy Sciences, U.S. DOE, under Contracts No. DE-AC02-05CH11231 and No. DE-AC02-76SF00515, respectively. The Stanford work is supported by the US DOE, Office of Basic Energy Science, Division of Materials Science and Engineering,

under award number DE-AC02- 76SF00515.

Author contributions

W.L., P.D., Z.X. and H.D. carried out the STM experiments; W.L. and Y.Z. performed the ARPES experiments; W.L., X.C. and Z-X.S. designed and coordinated the experiments; D.H.L. and M.H. provided experimental support at Stanford Synchrotron Radiation Lightsource. S.K.M. provided experimental support at Advanced Light Source. Y.Z., D.H.L. M.Y. and R.G.M. provided discussion about data and interpretation. Q-K.X. oversaw the project. W.L. wrote the manuscript with comments from all authors.

Additional information

The authors declare no competing financial interests.

Figure Captions

Figure 1| MBE film and C_2 domains of FeSe. a, Crystal structure of FeSe. **b**, STM topographic image of a FeSe film (150 nm × 150 nm, bias voltage V = -50 mV, tunneling current I_t = 100 pA). The maze-like patterns are C_2 domain walls between two neighboring nematic domains perpendicular to each other. **c,** stripes induced by impurities (70 nm × 70nm, 60 mV, 10 pA). The stripes are two-folded (marked by the white arrows), and rotated 90° when crossing the domain walls (the yellow dashed lines). From the inset (10 nm × 10 nm, 60 mV, 200 pA), the periodicity ~ 1.9 nm and orientation of the stripes could be determined. The apparent heights and contrasts of domain walls in **b** and **c** are different due to the different bias voltages applied (Supplementary Note 1). The periodicity of the stripes can also be extracted by fast Fourier transform of the real space images (Supplementary Note 2).

Figure 2 | Bias voltage dependence of the stripes in the vicinity of the impurities. **a-d**, STM topography of the stripes induced by four dumbbell-shaped impurities obtained with different bias voltages. The arrows highlight the stripes between two impurities and the color of the arrow denotes the stripes' phase change of 180°. The scan size of all images here is 25nm × 25 nm and the tunneling current is 100 pA.

Figure 3 | Charge ordering origin of the stripes. a, STM topography of the stripes near two impurities (20nm × 10nm, 60 mV, 200 pA), which is the area within the white dashed line in Fig. 2d. **b-p**, spatially resolved density-of-state maps at different energies obtained on the same area to **a**. Set point for **b-e** and **i-p**: V = 200 mV, I_t = 400 pA; Set points for **f-g**: V = 500 mV, I_t = 500 pA. The white and red arrows indicate the static stripes and the orange dashed curves highlight the quasiparticle interferences from low energy dispersive bands.

Figure 4 | Temperature dependence of the stripes and the C_2 domain walls. **a-d**, the C_2 domain wall (the yellow dashed lines) gradually disappears at elevated temperatures. C_2 domain walls could only be pinned near the defects as marked by red arrows in **c** at 120 K and completely disappear at 130 K in **d**. Set point: V = -60 mV, I_t = 6 pA. The stripes are absent at 77 K in **e**. In **f-h**, the stripes are clearly visible and the periodicity is independent of temperature from 60 K to 4 K. Set point for e-h: V = 60 mV, I_t = 6 pA. **i**, phase diagram based on temperature dependent measurements of

the stripes.

Figure 5 | The interaction between the stripes and the impurity states. a and **b**, distortion of the impurity states due to the interaction with CO. In **a** and **b**, the deflection angle of the "dumbbell" is larger than 10° at 4 K. While in **c**, the deflection angle of the "dumbbell" is negligible at 77 K when the CO is absent. Set points: V = 30 mV, I_t = 6 pA. **d**, schematic of the distortion at low temperature. The electronic states are elongated near E_F due to the large nematicity, and the impurity states tend to align with the stripes.

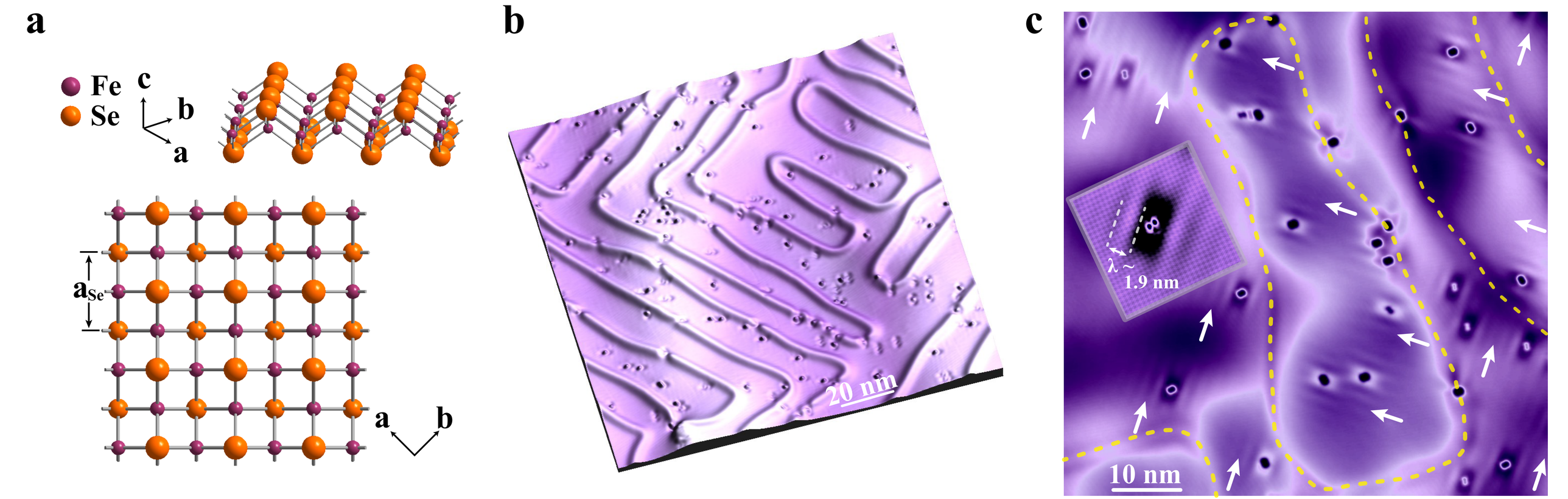
a
Fe
Se
c
b
a
a_{Se}
a
b
b
20 nm
c
λ ~ 1.9 nm
10 nm

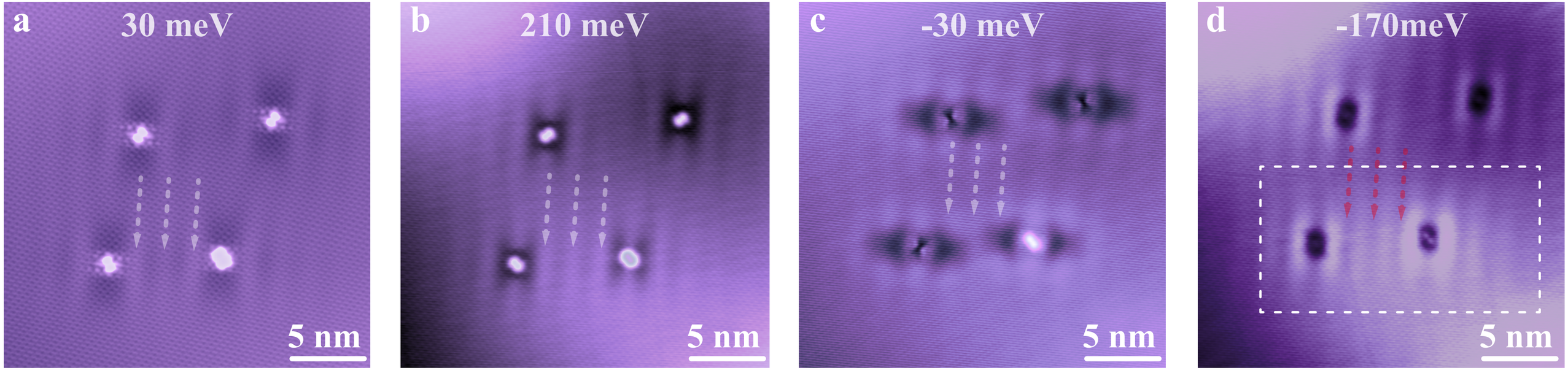
a
30 meV
5 nm
b
210 meV
5 nm
c
-30 meV
5 nm
d
-170meV
5 nm

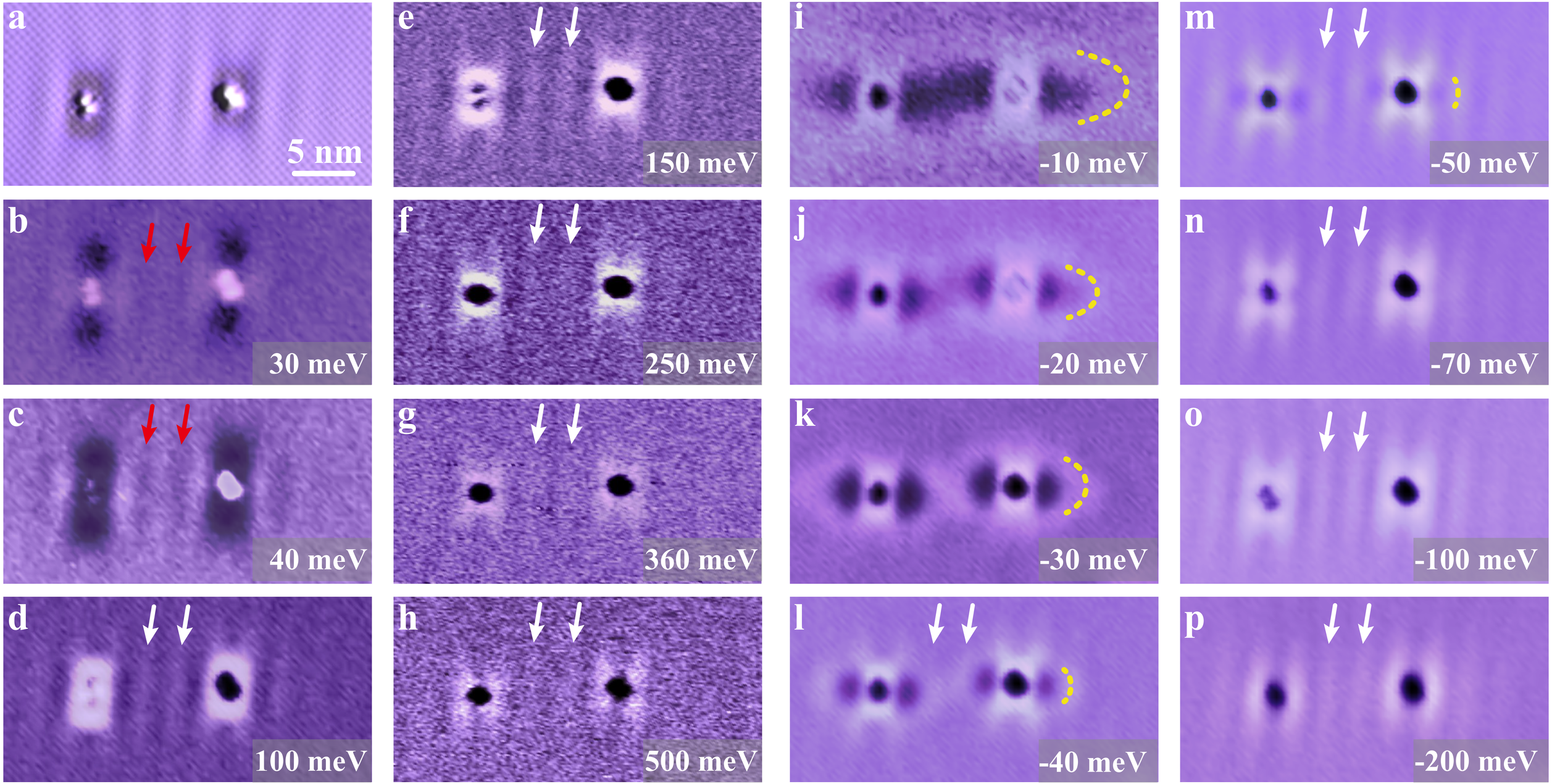
a
5 nm
b
30 meV
c
40 meV
d
100 meV
e
150 meV
f
250 meV
g
360 meV
h
500 meV
i
-10 meV
j
-20 meV
k
-30 meV
l
-40 meV
m
-50 meV
n
-70 meV
o
-100 meV
p
-200 meV

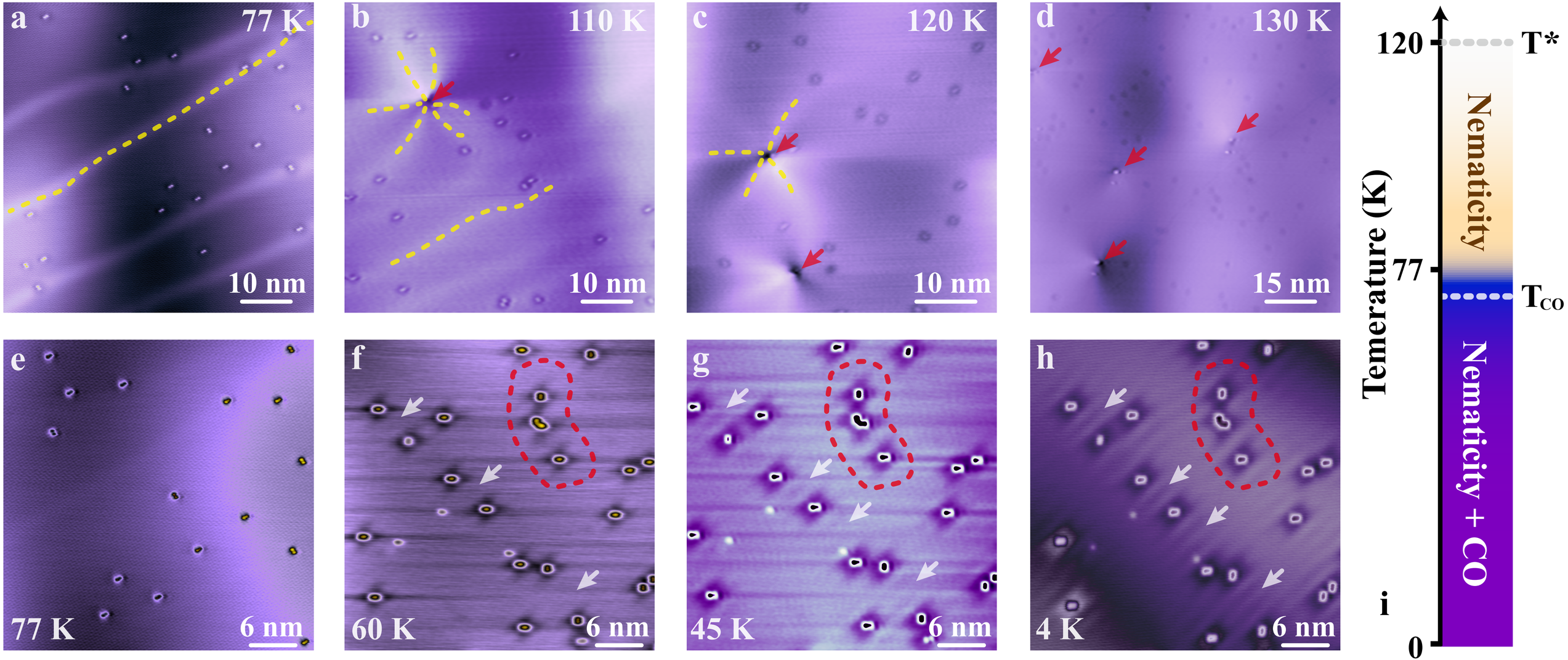
a
77 K
10 nm
b
110 K
10 nm
c
120 K
10 nm
d
130 K
15 nm
e
77 K
6 nm
f
60 K
6 nm
g
45 K
6 nm
h
4 K
6 nm
120
T*
77
Tco
i
0
Temerature (K)
Nematicity
Nematicity + CO

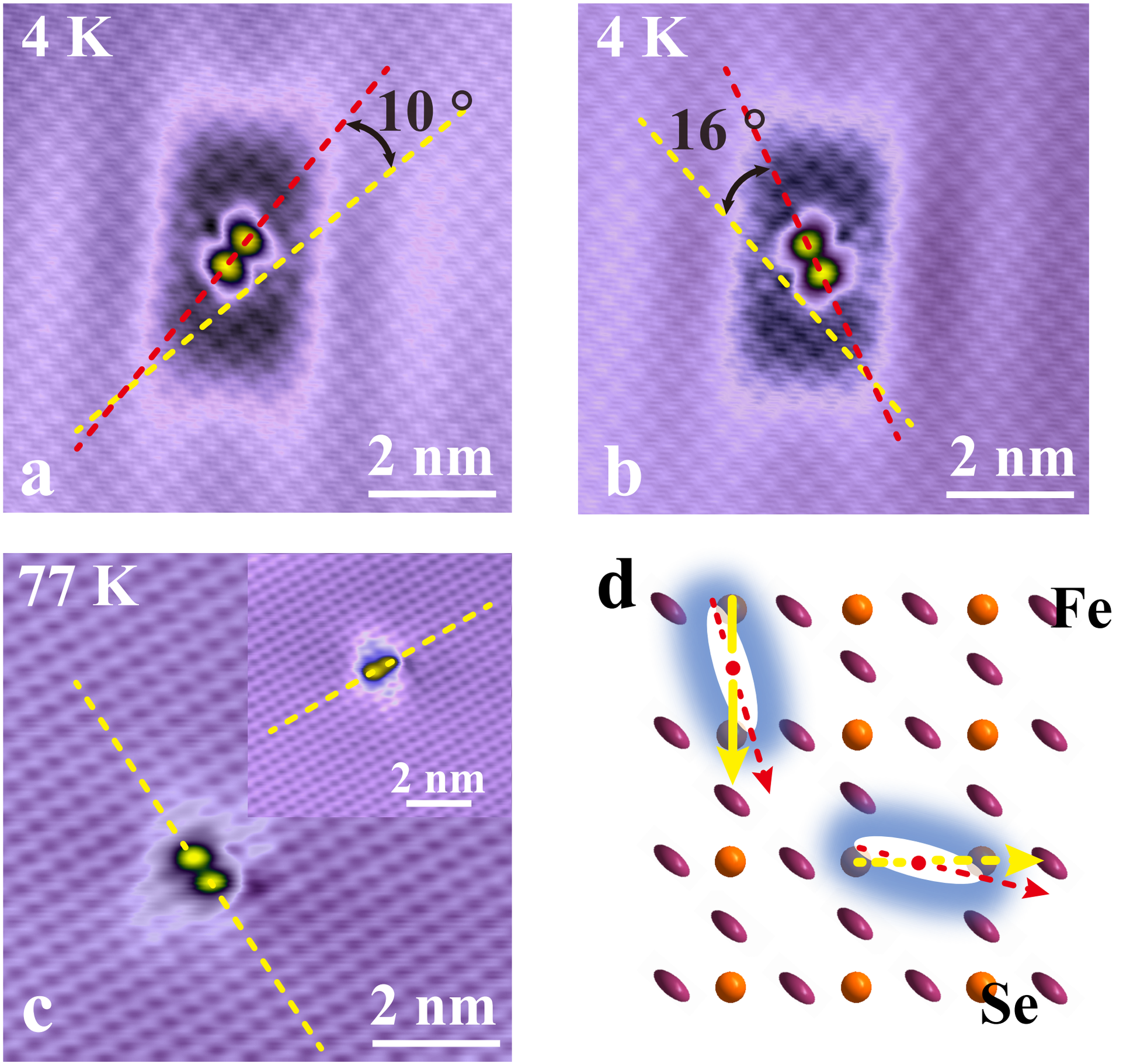
4 K
10 °
2 nm
a
4 K
16 °
2 nm
b
77 K
2 nm
2 nm
c
d
Fe
Se